128. Anderso.., C. C., and Hayes, F. N., *Annual Rev. of Nucl. Sci.*, (*Ann. Rev. Inc.*, Palo Alto, Calif.) 6, 303 (1965).
129. Freedman, A. J., and Anderson, E. C., *Nucleonics*, 10(8), 57 (1952).
130. Johnson, W. H., *Science*, 124, 801 (1956).
131. Watt, D. E., and Ramsden, D., *High Sensitivity Counting Techniques*, *Inter. Ser. of Monographs on Electronics and Instr.*, 20, Pergamon Press, London (1964).
132. Sugihara, T. T., *Low Level Radiochemical Separations* NAS-NS 3103 (1961).
133. Sugihara, T. T., *Radiochemical Separation of low-level Radioactivity*, *Progress in Nuclear Energy*, *Ser. IX* (*Anal. Chem.*) 3, part 1; Ed. C. E. Crouthamel, Pergamon Press (1962).
133b. De Voe, J. R., *Radioactive Contamination of Materials used in Scientific Research*, U.S. Natl. Acad. Sci., Natl. Research Council, Public no. 895 (1961).
134. *IAEA Symp.*, *Radioactive Dating and Methods of Low-Level Counting*; Vienna (1967).
135. Norton, E. F., *Chemical Yield Determinations*, NAS-NS-3111.
136. Cali, J. P., *Trace Analysis of Semiconductor Materials*, Pergamon Press, p. 59 (1964).
137. Kamemoto, Y., and Yamagishi, S. Y., *J. Chem. Soc. Japan, Pure Chem. Sec.* (Nippon Kagaku Zasshi), 84, 291 (1963).
138. Kamemoto, Y., and Yamagishi, S., *Bull. of the Chem. Soc. of Japan*, 36, 1411 (1963).
139. Heydorn, K., *Trans. Am. Nucl. Soc.*, 9, 70 (1966).
140. Morrison, G. H., Gerard, J. T., Travesi, A., Currie, R. L., Peterson, S. F. and Potter, N. M., *Anal. Chem.*, 41, 1633 (1969).
141. Filby, R. H., Haller, W. A. and Shah, K. R., *J. Radioanalyt. Chem.*, 5, 277 (1970).
142. Girardi, F., *Modern Trends in Activation Analysis*, NBS Special Public. no. 312, I, p. 577, Washington D.C. (1969).
143. Thompson, B., *Modern Trends in Activation Analysis*, NBS Special Public. no. 312, I, p. 634, Washington D.C. (1969).
144. May, S., and Pinte, G., *Modern Trends in Activation Analysis*, NBS Special Public. no. 312, I, p. 655, Washington D.C. (1969).
145. Baker, C. W., Brooke, N. M. and Goode, G. C., Paper presented at the 2nd S.A.C. Conference, Nottingham (1968).
146. Laul, J. C., Case, D. R., Wechter, M., Schmidt-Bleek, F. and Lipschutz, M. E., *J. Radioanalyt. Chem.*, 4, 241 (1970).
147. Allen, R. O., Haskin, L. A., Anderson, M. R. and Müller, O., *J. Radioanalyt. Chem.*, 6, 115 (1970).
148. Denechaud, E. B., Helmke, P. A. and Haskin, L. A., *J. Radioanalyt. Chem.*, 6, 97 (1970).
149. Tomura, K., Higuchi, H., Miyaji, N., Onuma, N. and Hamaguchi, H., *Anal. Chim. Acta*, 41, 217 (1968).
150. Graber, F. M., Lukens, H. R., and MacKenzie, J. K., *J. Radioanalyt. Chem.*, 4, 229 (1970).
151. Higuchi, H., Tomura, K., and Hamaguchi, H., *J. Radioanalyt. Chem.*, 5, 207 (1970).

CHAPTER 9

ANALYSIS WITHOUT CHEMICAL SEPARATION

I. General Principles

Activation analyses without chemical separations can be applied in special conditions only. In the most simple case the ratio of the activities induced in the matrix and in the element to be determined is low or even zero. If the matrix activity is low, chemical separations can be avoided for the analysis of minor constituents, but generally not down to the trace element level. Determinations even down to this level can be achieved when the matrix does not become radioactive. When the matrix activity is shorter lived than the activity induced in the element to be determined, the former can be allowed to die out before the latter is measured.

Even when a long-lived matrix activity is obtained, an attempt can be made to count the isotope to be determined in a selective way. This can be achieved either by discriminative counting, when the energy of the matrix activity is lower than the isotope of interest, or by the use of an instrumental technique, such as described in Chapter 6, section III, E, which can turn a detection method into a more or less selective one for a given isotope. Anyhow, with this last technique the difficulties generally increase rapidly when reaching the ppm level, due to the fact that the matrix/element activity ratio becomes quite high. This high matrix activity can give rise to saturation and pile-up in the detector and in the electronic measuring circuits. If one minor or trace element gives rise to an intense and high energy radiation, masking of low intensities at lower energies also becomes unavoidable.

Practically every measuring technique can be coupled to an analysis of a decay curve. This provides not only a purity check of the measured activity by half-life, but when interferences of the matrix or of impurities occur, an analysis of this curve can allow the determination of the activity of the isotope of interest. Here again, at the trace impurity level, activities are not normally large enough to allow a precise analysis of the curve, due to the large statistical fluctuation in count rate. The

eventual aim of nondestructive activation analysis is to save time and work, which is of interest when dealing with routine analysis of large amounts of samples. In this philosophy, fully automated activation analysis procedures have been developed. In this chapter, examples will be given of activation analyses without chemical separation and the applied techniques will be described. For convenience, the latter will be split into two groups: these based upon the nuclear properties of the radionuclide of interest and those based upon detection and measuring instrumentation. A survey of nondestructive activation analysis techniques is given by Adams and Hoste (1).

II. Techniques Based on Nuclear Properties

Under the nuclear properties of an isotope one can classify the type and energy of the emitted radiation, the half-life and the time correlation between the different radiation events. All these properties can be found in the decay scheme as described in Chapter 6, section I, B. The type of the emitted radiation mainly determines the choice of the detector, as is discussed in Chapter 6. The radiation energy of the isotope to be determined has to be considered in relation to the energy of the interfering activity. When the latter is the smallest one, a simple discriminative counting technique such as gamma spectrometry can be applied, as in Chapter 6.

The correlation between the different radiations, emitted by the same isotope, can be used as a guide to judge if coincidence techniques can be applied. For example, gamma-gamma and beta-gamma cascades, decaying over very short-lived energy levels, are excellently suited for coincidence purposes.

(A) Analysis of Complex Decay Curves

1. *General*

The determination of the half-life of a radioactive isotope offers an excellent criterion for identification, certainly in combination with a selection in nature and energy of the emitted radiation. Furthermore, the analysis of a decay curve permits a quantitative determination as the activity of the isotope of interest can be corrected in each point of the decay curve for shorter and longer lived activities and an extrapolation to the end of irradiation or to any convenient time can be performed.

Indeed, the decay of an active isotope is exponential, as described in Chapter 5, and is represented in the case of a single isotope, by

$$A(t) = A^0 \exp\left(-\frac{\ln 2}{T_{1/2}} t\right) \tag{9.1}$$

where $A(t)$ and A^0 are the activities respectively at a time t and at the end of irradiation. $T_{1/2}$ is the half-life.

A plot of the logarithm of $A(t)$ versus t yields a straight line. The intersection with the ordinate yields A^0 for $t = 0$, and the slope of the line allows calculation of the half-life. The total activity $A(t)_t$ of a complex decay curve with i components, measured at a time t, can be expressed as a sum of exponentials

$$A(t)_t = \sum_i A_i^0 \exp\left(-\frac{\ln 2}{T_{1/2i}} t\right) \tag{9.2}$$

and can be analyzed as such.

From this part of the curve, the half-life of the longest lived isotope can be determined and by extrapolation one can correct the shorter-lived activities for this contribution. This procedure is repeated for each of the present components.

The analysis can be performed either graphically or with the aid of a computer. In the first case, half-lives should differ by a factor of approximately 5, whereas in the second case a factor 2 or 3 can be sufficient to obtain good analysis. It is obvious that the feasibility of an analysis will also depend on the relative activities of the components and on the total activity of the measured sample. Decay curves, showing large statistical fluctuations, as can obtain when low count rates have to be measured, are indeed very tedious to analyze. A smoothing procedure of the experimental points can greatly facilitate the analysis. Computer programs for the analysis of complex decay curves are described in the literature (2,3,4,5,6,7,8). They are based on a least squares fit or on a Fourier style analysis of the data.

The decay curve analysis is very well suited to the determination of short-lived isotopes, implying short irradiation and measuring times and thus very rapid procedures. When the isotope of interest is easily measured, an integral counting method can be sufficient. In all other cases discriminative counting, gamma spectrometry, or even

special measuring techniques can be used. The data coming from this equipment are generally fed into a multiscaler which can be either a printing scaler, provided with two chronometers, one for measuring time and one for waiting time, or a multichannel used in the multiscaler mode.

When measuring short half-lives, care has to be taken in the choice of the duration of the measurement of a single point with respect to the half-life as is described in Chapter 11, section V, B. Indeed, significant extrapolation errors can occur when the measuring time is large in comparison with the half-life.

2. *Examples*

Some typical examples of nondestructive activation analysis by means of decay curve analysis are:

(a) Aluminium and chlorine in terphenyl. Aubouin (9) describes a method for the determination of aluminium and chlorine in terphenyl or other organic matrices. The nuclides ^{28}Al (E_γ = 1.78 MeV, $T_{1/2}$ = 2.27 m) and ^{38}Cl (E_γ = 1.64–2.15 MeV, $T_{1/2}$ = 37 m) formed by (n, γ) reaction, are used for the determination, performed by gamma spectrometry coupled to decay analysis.

This permits us to take into account the interfering activities of the isotopes ^{24}Na (E_γ = 1.38–2.7 MeV, $T_{1/2}$ = 15 h) and ^{56}Mn (E_γ = 0.84 MeV, $T_{1/2}$ = 2.6 h) in the chlorine determination, as can be seen from Figure 9.1, where a decay curve of a typical sample is given.

The limits of this method are of course dependent on the interfering activities but for chlorine e.g. 5×10^{-7} g can be stated as normal.

(b) Indium in zinc. Gibbons and Lawson (10) determined indium in zinc and zinc alloys by means of the decay curve analysis of the activity under the 1.27 MeV photopeak of ^{116m}In ($T_{1/2}$ = 54 m). In this way the authors could correct for the interferences of the 1.11 MeV photopeak of ^{65}Zn, and were able to perform the analysis without chemical separation.

(c) Silver in lead. Adams *et al.* (11) determined silver in lead without chemical separation by decay curve analysis of the activity due to ^{110}Ag ($T_{1/2}$=24.2 s), which is formed from natural silver by (n, γ) reaction. Use was made of the fast pneumatic transfer system at BR–1 of the S.C.K. at Mol (Belgium) (transfer time = 0.2 s). A NaI(Tl) crystal coupled to a single channel ensured the selection of the ^{110}Ag 0.66 MeV photopeak, and a 400 channel multiscaler recorded the decay curve of the measured activity. Standards and samples were irradiated separately, together with a platinum flux monitor. According to this method, silver contents down to 0.02 μg were determined in 0.5 to 1 g lead samples, with a reproducibility better than 10%. Interferences due to copper and antimony, which also give rise to short-lived isotopes, could not be detected, even when these elements were present in an excess of 50 times the silver content.

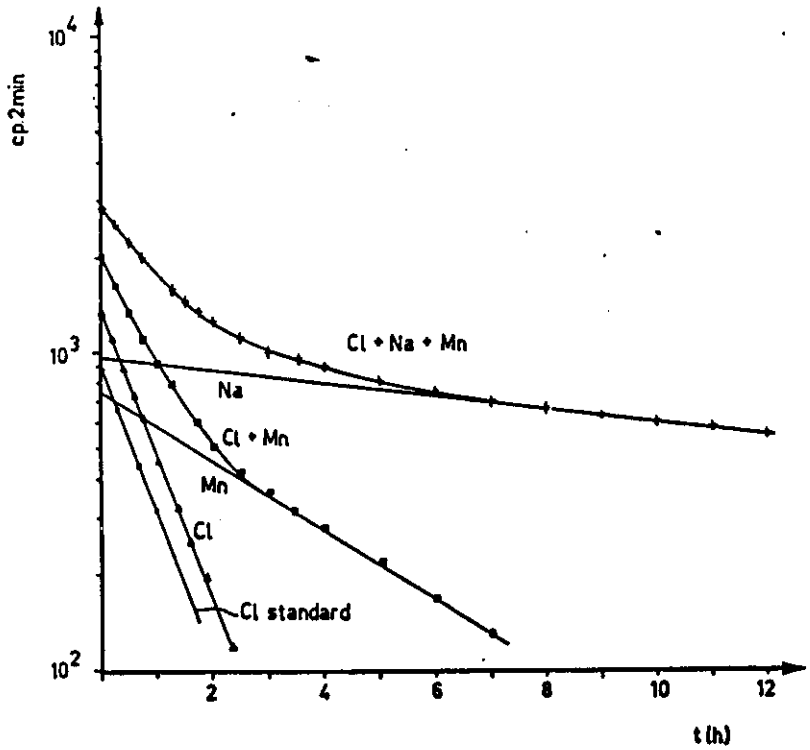

Fig. 9.1. Decay curve of chlorine in a terphenyl sample containing Na and Mn (9).

(B) Coincidence Techniques

1. *General*

The principles and the apparatus concerning coincidence techniques, including beta-gamma, gamma-gamma, and gamma-sum coincidence, have been described in Chapter 6, section III, E, 1.

The main parameters of this method are situated not only in the time correlation between the components of the considered cascade, but also in the energy of these radiations. For this reason, energy selection coupled to time selection will yield the best results. Furthermore, coincidence methods are not only important because of the specificity of the counting technique, but are sometimes used for the sake of sensitivity, even after chemical separation.

In the first case, the aim will be to minimize the random coincident events due to the activity of the matrix and possible impurities, whereas in the second case a coincident background must be obtained as low as possible in order to ensure a high signal/background ratio.

The total measured coincident count rate R_t is given by:

$$R_t = R_c + R_r + R_B \tag{9.3}$$

where R_c, R_r and R_B represent respectively the true coincident count rate due to the measured cascade (see equation (6.49)), the random coincident rate due to the matrix and impurities (see equations (6.50) and (6.52)) and the background coincident rate.

From equation (9.3) R_c can be evaluated, after calculation of R_r by means of equation (6.50) and after measurement of R_B.

The coincident background rate, R_B, cannot be treated simply as a random coincidence, but can be regarded as composed of three effects: a time coincident part, coming from cosmic radiation and possibly from the electronic circuitry, a random coincident part and a part produced by scattering of radiation from one detector into the other.

For two unshielded detectors, very close together, the scatter contribution is about one order of magnitude larger than the true coincident part, which is in turn about one order of magnitude larger than the random coincidences. The scatter contribution can be minimized by separating the two detectors from each other, or by placing them at an angle and inserting a lead wedge between them. This last solution cannot be adopted when strong angular correlations exist, as is the case

with annihilation gamma rays. It has to be noted that the same scatter phenomenon can occur with the matrix and impurity activities, when the detectors are placed close together. In activation analysis, one will have to compromise, since removing detectors from the source means a decrease in counting efficiency and very long counting times, especially when dealing with trace analysis.

Although the contribution of the true coincident component in the background cannot be avoided, as appears from equation (6.49), the effect can be minimized by adequate shielding. A reduction in background from 0.12 cpm to 0.035 cpm has been reported (12) for the counting of ^{75}Se with a 265–280 keV gating pulse in coincidence with the 121–136 keV region, by moving the detectors, placed as closely together as possible, from a 50 × 50 × 50 cm lead shield with a 5 cm wall thickness into a 100 × 100 × 100 cm one, with walls of 10 cm thickness. The random coincident background can also be lowered, by reducing the resolving time, as can be seen from equation (6.52).

The contribution of R_r is negligible when a pure background is measured, but is the most important one when matrix and impurity activities are present. Let the total sample disintegration rate D_t be composed of the disintegration rate of the element to be determined D_e and of the impurities and matrix disintegration rate D_i. According to equations (6.49) and (6.52) one can write, after background subtraction:

$$\frac{R_c}{R_r} = \frac{D_e}{2\tau D_e^2} = \frac{D_e}{2\tau(D_e + D_i)^2} \tag{9.4}$$

In general $D_e \ll D_i$, which simplifies equation (9.4) to

$$\frac{R_c}{R_r} = \frac{D_e}{2\tau D_i^2} \tag{9.5}$$

Assuming a resolving time of 0.010 μs, it is easily shown that equal coincident and random count rates are obtained for a disintegration rate in matrix and impurities of $7 \times 10^3 (D_e)^{1/2}$. This means that a given element can still be determined, when the accompanying activities are a factor of $7 \times 10^3 (D_e)^{1/2}$ times larger than its own activity.

2. *Examples*

(a) Borg, Segel, Kienle and Campbell (13) applied a beta-gamma coincidence technique for the nondestructive determination of man-

ganese in biological material. The nuclide ^{56}Mn has indeed a prominent gamma ray at 0.85 MeV, which is coincident with a beta ray of 2.85 MeV maximum energy. In biological material however, an activity several orders of magnitude larger than the ^{56}Mn activity is obtained, due to ^{24}Na, emitting two gamma rays at 1.38 and 2.76 MeV respectively whereas the maximum energy of the beta ray is 1.37 MeV.

The normal beta-gamma technique, using lower energy discrimination for the beta rays, could not be applied, as the detector is also for a small percent sensitive to gamma rays. Therefore selection of the pulses from the plastic beta detector became necessary and was performed by means of a telescope counter inserted between the source and the plastic detector. This counter consists of a very thin plastic scintillator, which is practically transparent for gamma rays, whereas beta rays lose part of their energy in it before reaching the main beta detector, where they are stopped. The light pulses obtained with the telescope detector are seen by a photomultiplier by means of an aluminized mylar reflection box and brought into coincidence with the pulses stored in the main beta detector. The coincident output of the beta detectors is subsequently brought into coincidence with the gamma rays, measured with a sodium iodide crystal. Figure 9.2 shows a scheme of the apparatus and a normal gamma spectrum in comparison with a triple coincident spectrum of a ^{56}Mn–^{24}Na mixture. Furthermore, the authors made use of selective activation, obtained by surrounding the sample with 93% ^{10}B enriched boron powder, enhancing in this way the resonance to thermal activation of ^{55}Mn. Manganese to sodium concentration ratios of 10^{-6} were analyzed without chemical separation.

(b) Hecker and Herr (14) applied the two channel gamma-gamma coincidence method for the determination of traces of hafnium in zirconium. Thermal neutron activation gives rise to the isotope ^{181}Hf ($T_{1/2}$ = 45 d), whereas ^{95}Zr ($T_{1/2}$ = 65 d) and ^{97}Zr ($T_{1/2}$ = 17 h) are obtained from the matrix. The decay scheme of ^{181}Hf shows a gamma ray cascade with respective energies of 0.48 MeV and 0.14 MeV, whereas no cascades occur in the decay of both zirconium isotopes. Each channel was tuned to one of the cascade energies, and down to 5 ppm hafnium in samples of about 30 mg zirconium was determined without chemical separation. The authors claim that by optimizing irradiation time and sample size this limit can be lowered by a factor of 100. From the analysis of a zircaloy sample containing 57 ppm

Hf it appeared that no interferences occurred from Sn, Cr, Fe and Ni, which were present in respective concentrations of 1.5, 0.11, 0.10 and 0.03%.

(c) The applicability of the gamma-gamma coincidence technique, even when dealing with adjacent gamma rays, was demonstrated by Salmon (15). When cobalt has to be determined in an iron matrix by

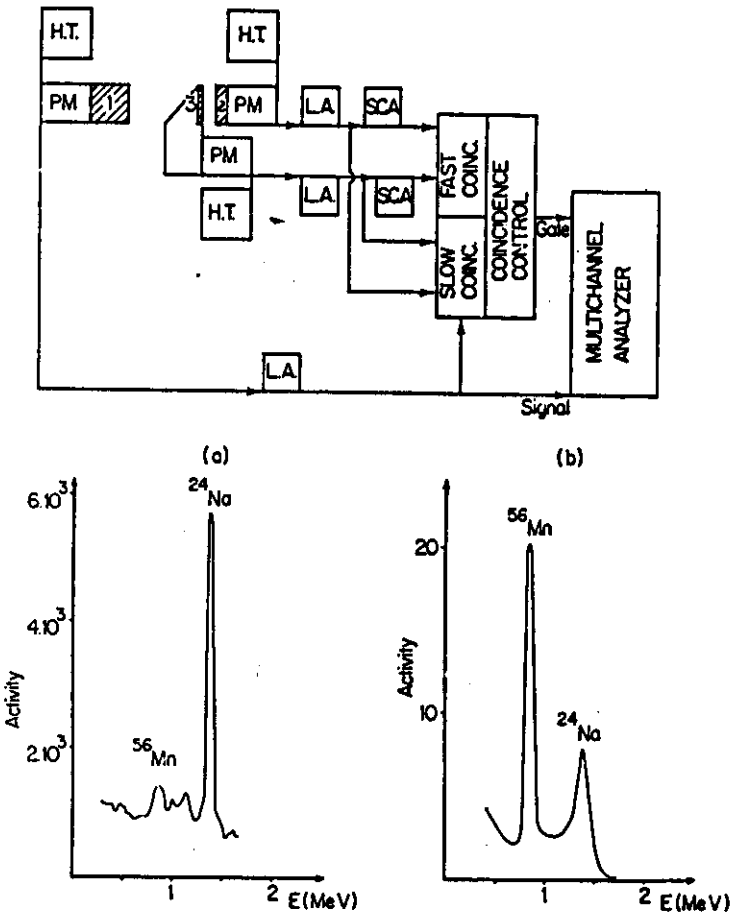

Fig. 9.2. Principle scheme of the β–γ triple coincidence gamma-spectrometer, according to Borg *et al.* Classical gamma-spectrum of a ^{24}Na–^{56}Mn mixture (a) and triple coincident spectrum of the same mixture (b) (13).

neutron activation analysis, the isotopes ^{60}Co ($T_{1/2}$=5.2 y) and ^{59}Fe ($T_{1/2}$=45 d) are formed. Both isotopes emit gamma rays of approximately the same energy: ^{60}Co 1.17 and 1.33 MeV and ^{59}Fe 1.10 and 1.29 MeV. With a NaI(Tl) detector, both spectra cannot be separated. From the decay scheme, it appears however that the ^{60}Co gammas are emitted in cascade, whereas the ^{59}Fe ones are not. Thus, using a dual channel coincidence technique the ^{60}Co spectrum can be measured without interference from the ^{59}Fe activity, even when the latter is 25 times larger than the cobalt activity, which is about the case when dealing with a steel sample containing 100 ppm cobalt.

(d) The same technique was used by Kim and Hoste (16) for the simultaneous determination of silver and antimony in bismuth, by means of the neutron produced isotopes ^{110m}Ag and ^{124}Sb. For ^{110m}Ag the 0.65 and 0.88 MeV gamma cascade was measured, whereas ^{124}Sb was determined using the 0.60 and 1.7 MeV cascade. In order to correct for the mutual interferences of both isotopes, two measurements were performed, one with both channels tuned in on the ^{110m}Ag cascade followed by a measurement with both channels tuned in on the ^{124}Sb cascade. By repeating these measurements with pure ^{110m}Ag and ^{124}Sb standards, the silver and antimony content in bismuth could be determined without chemical separation. When 1 g samples were irradiated at a neutron flux of 4×10^{11} n cm^{-2} s^{-1} for 25 days, the sensitivity of the method was in the ppb region.

(e) Adams and Hoste (17) used a coincidence technique for the nondestructive determination of tungsten and arsenic in vanadium pentoxide. The isotope ^{187}W, formed by (n, γ) reaction, was measured by means of the 72 keV–134 keV gamma cascade, where both gamma rays are strongly converted, giving rise to the 60 keV Re K-X-ray. These X-rays were measured in coincidence, making use of a NaI(Tl) wafer and a 3″ × 3″ NaI(Tl) detector, as described in Chapter 6, section III, D. The 68 keV Pb X-ray was reduced by lining the lead shield with cadmium and copper foil, and concentrations down to 200 ppb tungsten were determined in 200 mg V_2O_5 samples. Activities due to ^{76}As, ^{24}Na and ^{122}Sb interfere for 100%, when they are present in an excess of respectively 450, 1250 and 900 in comparison to the tungsten activity.

Arsenic was determined subsequently, using a dual channel gamma-gamma coincidence spectrometer. The 0.56–0.66 MeV gamma cascade of ^{76}As was used for this purpose, and allowed 10 ppm arsenic to be

determined in the 200 mg V_2O_5 samples. Activities due to tungsten, gold, platinum, iridium and molybdenum do not interfere, whereas an excess antimony activity could cause some errors. A correction for the ^{24}Na activity which interferes through the 1.37–2.76 MeV gamma cascade can be made if required, by a subsequent measurement of the 1.37 MeV gamma peak.

(f) It is evident that when dealing with positron emitters, use can be made of a gamma-gamma coincidence counting technique of both 0.511 MeV annihilation gamma rays. These gamma rays show a particularly strong angular correlation, since they are emitted at 180° angles. Wölfle, Herpers and Herr (18) made excellent use of this property in order to obtain additional selectivity when counting positron annihilation radiation in a gamma ray background, even when containing gamma-gamma cascades, which show negligible angular correlation. A simplified but nevertheless useful picture of the source–detectors assembly, is represented in Figure 9.3, where both NaI(Tl) crystals with a radius r, are of small thickness, and totally absorb the incident gamma ray. The distance of the source P from both detectors is to a good approximation equal to R. When P is a source, emitting a nonangular correlated gamma cascade, with a disintegration rate D_c, the coincidence count rate R_c, will be given by

$$R_c = D_c\left(\frac{r^2\pi}{4R^2\pi}\right)^2 \tag{9.6}$$

when the cross section AC is said to be equal to the spherical surface ABC, which is approximately true when R is large.

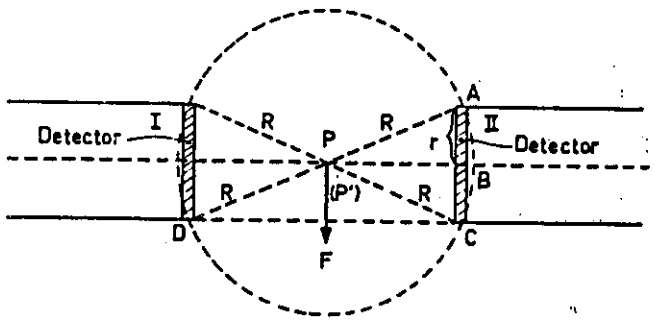

Fig. 9.3. Detector set up for coincidence calculations according to Herr *et al.* (18).

On the other hand, when P is replaced by 180° correlated positron annihilation source P′, the coincidence count rate R'_c will be

$$R'_c = D'_c\left(\frac{r^2\pi}{4R^2\pi}\right) \tag{9.7}$$

where D'_c is the disintegration rate of the source P′.

From equations (9.6) and (9.7) it appears that the coincident count rate for a noncorrelated radiation decreases with R^4, whereas a 180° correlated one decreases only with R^2. This implies that the source–detector distance R has to be quite large, in order to suppress the uncorrelated gamma background, when measuring positron annihilation rays. At the same time, the random coincidence rate is also decreased, as appears from equation (6.50). As an example, Figure 9.4 shows the ratio of the coincidence count rate to the single channel count rate as a function of R for the isotope ^{22}Na. Curve A is drawn for the 0.511 MeV positron annihilation radiation, curve B for the 0.511–1.27 MeV gamma-gamma coincidence. Both curves are normalized

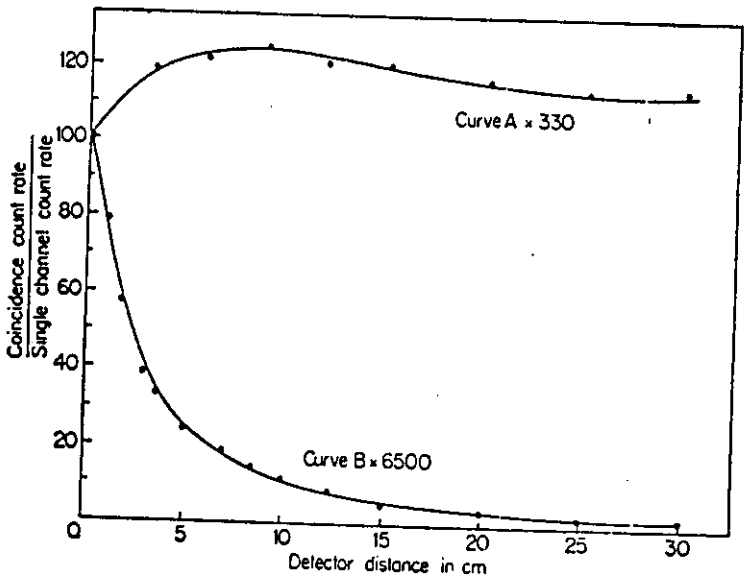

Fig. 9.4. Ratio of coincident to single channel count rate versus the distance of the detectors. Curve A: 180° correlated γ–γ coincidence (^{22}Na 0.51/0.51 MeV). Curve B: uncorrelated γ–γ coincidence (^{22}Na 0.51/1.28 MeV) (18).

by multiplying by a factor of 330 and 6500 respectively. From figure 9.4 it appears that the noncorrelated gamma-gamma coincidence background can be reduced by a factor of 10^3.

A further advantage when dealing with positron emitters, exists in the possibility of measuring separately the total coincidence count rate of the source and the sum of the uncorrelated coincidence rate and the random coincidence rate. For this purpose the source is measured once in position P and once in position F, which is located slightly over the line DC, as is shown in Figure 9.3. With the source at F, the 180° correlated radiation count rate is decreased to a fraction of 0.007. This is negligible in comparison with the interfering count rate, which is still recorded, as R remains practically unchanged by the source displacement, especially when R is large. As an example, when dealing with 7.5 cm diameter detectors and R = 30 cm, the source displacement causes a change in R of only 0.9%.

The authors used this technique for the nondestructive determination of copper in Bi, Pb, Tl, Be, Se, Sn, Al and iron meteorite by means of the ^{64}Cu isotope, which is mainly a positron emitter.

Only the matrices Se and Sn give rise to measurable interferences, which could be corrected for by half-life determination. The limit of the method is situated at about 6 ppb Cu for 1 g samples. Possible interferences indicated by the authors are summarized in Table 9.1. For the copper determination in bismuth, the authors found that for the interfering isotopes ^{198}Au, ^{110m}Ag, ^{76}As and ^{122}Sb, a 40 times larger activity can be tolerated than by the gamma-gamma coincidence method, used for the same analysis by Kim, Speecke and Hoste (19).

(g) The gamma sum coincidence method has been used by Adams and Hoste (20) for the determination of antimony in lead without chemical separation. The authors made use of the 0.603–1.69 MeV gamma-gamma cascade of ^{124}Sb, the sum peak of which is situated at 2.29 MeV. The samples were disks of about 3 g lead with a thickness of about 3 mm, in order to avoid measurable absorption of the gamma rays. After a 4 day cooling period, the only remaining interference was due to ^{110m}Ag, which emits gamma rays up to 2.29 MeV. A correction for this interference was obtained by measuring the activity between the two ^{124}Sb photopeaks, which was indeed entirely due to the silver activity and comparison with a pure ^{110m}Ag standard. The limit of the method was situated at 10^{-3} μg antimony.

(h) Wahlgren, Wing and Hines (21) applied the sum coincidence

Moreover, it can be shown that the standard deviation of $s_{(x_j)}$ on x_j is given by

$$s_{(x_j)} = \left[\frac{S}{n-m}(a_{jj})^{-1}\right]^{1/2} \tag{9.31}$$

where $(a_{jj})^{-1}$ is the corresponding diagonal element of the inverse matrix $|a|^{-1}$.

From a complex spectrum and from the spectra of the composing standards one can compute the best values for the ratios of each component to its respective standard and also the standard deviation. As all channels of the spectrum are used, statistical counting errors are minimized. Moreover, no subjective errors are induced. One should however remark that the generation of random sumpeaks in the complex spectrum can seriously affect the results of this method, unless they are corrected for (36). Moreover, overlooking one component, or taking a standard into account missing in the complex spectrum, can give rise to serious errors in the computed ratios.

3. *Decay Curve Analysis*

As already mentioned in section II, A, complex decay curves can readily be analyzed by means of a computer, avoiding the time consuming graphical analysis and errors induced by subjective judgement.

The first and most simple way to analyze complex decay curves is to proceed according to the graphical method, using the least squares technique. A linear least squares fit is performed, starting with the interference free activity due to the longest lived isotope. In each point of this part of the decay curve, one can write:

$$\ln A^0 - \lambda t_i - \ln A_{i,i} = Z_i \tag{9.32}$$

where A^0 represents the activity of the considered isotope at time zero (usually at the end of the irradiation), $A_{i,i}$ its activity after a decay time t and λ the disintegration constant. The error, due to the counting statistics, is denoted as Z_i. Writing equation (9.32) for n interference free points, and summing the squares, yields:

$$\sum_{i=1}^{n}(\ln A^0 - \lambda t_i - \ln A_{i,i})^2 = \sum_{i=1}^{n} Z_i^2 \tag{9.33}$$

By equating the partial derivatives of (9.33), with respect to $\ln A^0$ and λ, to zero and solving the set of equations one obtains estimates for A^0 and λ for the considered isotope. Starting with the points representing the activity of the isotope having the smallest decay constant, the program is iterated with increasing n, until A^0 and consequently λ increase. The foregoing values are then taken as the best estimates, by means of which the activity of the longest lived isotope is calculated and subtracted from each point of the decay curve. With this corrected decay curve, the program is started over again, in order to calculate the A^0 and λ of the next longer lived isotope, and so on.

It has to be remarked, that due to statistical fluctuations, the half-lives and the A^0 values found can differ from the correct ones (33). Therefore one considers the best values as follows

$$\begin{aligned} A_j^{0*} &= A_j^0 + \Delta A_j^0 \\ \lambda_j^* &= \lambda_j + \Delta\lambda_j \end{aligned} \tag{9.34}$$

where the asterisk indicates the best value and j indicates the different isotopes present in the complex decay curve. Now, the relation of the decay curve can be written:

$$A_i = \sum_j (A_j^0 + \Delta A_j^0)\exp[-(\lambda_j + \Delta\lambda_j)t_i] \tag{9.35}$$

where A_i indicates the total activity of the curve at t_i. Linearization of equation (9.35), in order to compute the optimum values for ΔA_j^0 and $\Delta\lambda_j$ by the least squares method yields:

$$\sum_i \left[\sum_j (A_j^0 + \Delta A_j^0 - A_j^0\Delta\lambda_j t_i)\exp(-\lambda_j t_i) - A_i\right] = \sum_i Z_i \tag{9.36}$$

This approximation is valid, because $\Delta\lambda_j t_i \ll 1$ and $\Delta A_j^0\Delta\lambda_j t_i \ll A_j^0$.

Minimizing the square of equation (9.36) by partial differentiation with respect to ΔA_j^0 and $\Delta\lambda_j$, and solving the set of equations thus obtained, yields the optimum values for ΔA_j^0 and $\Delta\lambda_j$ and hence the best values for A_j^{0*} and λ_j^*.

The program "SMASH" (Systematic Mathematical Analysis of "Short" Half-lives) (8, 41, 42) makes use of two separate mathematical procedures for complex decay curve analysis, which can be represented as a set of observations of the form:

$$A_i = \sum_j A_j^0 \exp(-\lambda_j t_i) \tag{9.37}$$

where A_i = total activity at time t_i

A_j^0 = initial activity of component j, with a decay constant λ_j.

The best value for A_j^0 and λ_j have to be selected in order to fit the n observations of the decay curve. This is obtained by a combination of the linear least squares technique and a direct search procedure. Values for λ_j are assumed, e.g. by graphical estimation, which are not to be the exact ones and are kept constant for the calculation of the first approximated values of A_j^0. This reduces equation (9.37) to a linear equation in A_j^0 and the least squares technique can be applied, minimizing with respect to A_j^0 the expression

$$\sum_i W_i (A_i - \sum_j A_j^0 k_{i,j})^2 = \sum_i Z_i^2 \tag{9.38}$$

where the weight W_i is assumed to be $1/\sigma_i^2$, σ_i^2 being the variance of the ith observation. $k_{i,j}$ is a storage matrix of exponentials. From this the quantity $\sum_j Z_i^2$ can be calculated, which is divided by the number of degrees of freedom (here number of observations minus number of components). The square root of this result is called FIT-1.

Now, the "pattern search" optimizes the parameters λ_j and A_j^0 of the function according to a direct search optimization scheme, without the use of derivatives. The variable FIT is chosen as the quantity to be optimized. The well known decay constants are fed into the program as constant, whereas the unknown ones are treated as variables. One should remark that it is always advantageous to keep the number of variable decay constants as small as possible. According to this, the first variable decay constant is changed by a preset increment, a new set of A_j^0's and a new FIT value is computed. This new value is compared with FIT–1 and if improvement is obtained, the decay constant is changed again, in the direction found (positive or negative) according to a certain pattern, until no further improvement occurs. Then a new direction or smaller increments will be chosen, until one of the convergence criteria is reached:

—further improvement of FIT is less than 10^{-6};

—the step size has been reduced 5 times;

—the total number of steps per parameter is larger than 400.

If no improvement is obtained by the first change of decay constant, the opposite direction is tried. The pattern search is subsequently repeated for all variable decay constants.

As the lowest value for FIT will not necessarily coincide at the true half-lives, the authors recommend performance of the final calculation of A_j^0, using the half-lives given in the literature, or obtained by a separate measurement of the pure isotopes. With these constant values, A_j^0 can be calculated without difficulties, even if the half-lives are as close to each other as 10–20%. For each A_j^0 the standard deviation can be computed according to

$$\sigma(A_j^0) = \text{FIT}\,[k_{j,j}^{-1}]^{1/2} \tag{9.39}$$

where $k_{j,j}^{-1}$ represents the corresponding diagonal element of the invert matrix, used for the calculation of A_j^0 by the least squares technique.

When the estimated number of components of the decay curve is too small, the program will end up with a high value of FIT and a warning message can be given. When on the other hand the estimated number of components is too large, several possibilities exist:

a negative A_j^0 value can be found for the extra component;

an exceptionally high standard deviation can be found for the A_j^0 value of the particular component;

a very low positive value for A_j^0 might even occur.

An example of a decay curve analysis using this program is given in Table 9.5. The half-lives of the known components are 2.5 m, 35.0 m and 316.5 m. Possibly one or two additional components can occur with respective half-lives of 10.0 and 80.0 minutes.

A more sophisticated way to solve complex decay curves, as represented by equation (9.37) is described by Gardner *et al.* (5). The function A_i (9.37) may be expressed in the form of a Laplace integral equation:

$$A_i = f(t) = \int_0^\infty \exp(-\lambda t)\, g(\lambda)\, d\lambda \tag{9.40}$$

where $g(\lambda)$ is a sum of delta functions. A plot of $g(\lambda)$ versus λ appears as a frequency spectrum, due to the statistical deviations on $f(t)$ and the numerical computation involved in determining $g(\lambda)$. An example of a plot of $g(\lambda)/\lambda$ versus λ for a four component decay curve is given in Figure 9.14. From these results it is clearly shown that a peak in the frequency spectrum indicates the presence of a component. The abscissa value at the centre of the peak gives the decay constant λ, whereas the height of the peak is proportional to A_j^0. The fluctuations around the zero ordinate can be puzzling as a low activity component could be overlooked. The authors perform the determination of $g(\lambda)$ from the experimental function $f(t)$, by inversion of the Laplace integral equation (9.40) using a method of Fourier transforms.

TABLE 9.5

Example of decay curve analysis using program "SMASH" (8)

Run	Component	Input half-life* (minutes)	Final half-life (minutes)	A_j^0 (cpm)	Final FIT
1	1	− 35.0000	28.2331	31289.203	3.619714
	2	− 2.5000	4.7385	107874.125	
	3	−316.5000	300.9714	2179.408	
Warning: number of components is probably too small					
2	1	− 80.0000	283.6895	−134.296	0.927518
	2	− 2.5000	2.5121	100083.500	
	3	− 10.0000	10.0281	49694.371	
	4	− 35.0000	35.1406	19943.469	
	5	−316.5000	316.5042	2120.122	
Warning: number of components is probably too large					
3	1	2.5000	—	100228.562	0.935111
	2	35.0000	—	20012.785	
	3	316.5000	—	2003.538	
	4	10.0000	—	49795.316	
4	1	− 2.5000	2.5119	100094.125	0.925820
	2	− 35.0000	35.1406	19940.410	
	3	−316.0000	318.6675	1986.785	
	4	− 10.0000	10.0289	49696.102	

* Negative sign indicates that half-life is considered as variable.

Firstly the variables of equation (9.40) are transformed into:

$$\lambda = \exp(-y) \quad \text{and} \quad t = \exp(x) \tag{9.41}$$

which yields, after multiplication of both sides by $\exp(x)$:

$$\exp(x)\, f[\exp(x)] = \int_{-\infty}^{\infty} \exp[-\exp(x-y)] \exp(x-y)\, g[\exp(-y)]\, dy \tag{9.42}$$

Denoting the Fourier transform of $\exp(x)\, f[\exp(x)]$ by $F(\mu)$, one obtains:

$$F(\mu) = [1/(2\pi)^{1/2}] \int_{-\infty}^{\infty} \exp(x)\, f[\exp(x)] \exp(i\mu x)\, dx \tag{9.43}$$

By combining equations (9.42) and (9.43) and rearranging terms, one can write:

$$F(\mu) = [1/(2\pi)^{1/2}] \int_{-\infty}^{\infty} g[\exp(-y)] \exp(i\mu y)\, dy \times \int_{-\infty}^{\infty} \exp[-\exp(s)] \exp(s) \exp(i\mu s)\, ds \tag{9.44}$$

where $s = x - y$.

The function $g\,[\exp(-y)]\, dy$ is related to the original variables as follows:

$$g\,[\exp(-y)]\, dy = g(\lambda)/\lambda\, d\lambda \tag{9.45}$$

Inspecting equation (9.44) one remarks that the right hand side is the product of $G(\mu)$, which is the Fourier transform of $g\,[\exp(-y)]$,

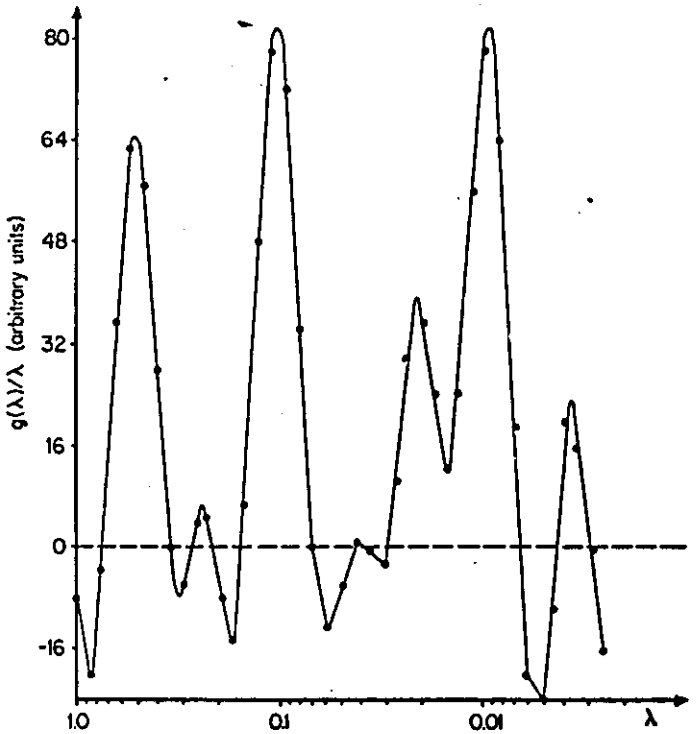

Fig. 9.14. Analysis of a four component decay curve with $\lambda_1 = 0.5$; $\lambda_2 = 0.1$; $\lambda_3 = 0.02$ and $\lambda_4 = 0.01$ (5).

and $K(\mu)$, which represents the Fourier transform of exp $[-\exp(s)]$ exp (s).

According to this, equation (9.44) can be written:

$$F(\mu) = (2\pi)^{1/2} G(\mu)\, K(\mu) \tag{9.46}$$

from which:

$$G(\mu) = [1/(2\pi)^{1/2}]\, [F(\mu)/K(\mu)] \tag{9.47}$$

Writing the inverse Fourier transform of $G(\mu)$, one eventually finds:

$$g\,[\exp(-y)] = (1/2\pi) \int_{-\infty}^{\infty} [F(\mu)/K(\mu)] \exp(iy\mu)\, \mathrm{d}\mu \tag{9.48}$$

It is obvious however that equations (9.43) and (9.48) cannot be numerically integrated from $-\infty$ to ∞. So, by introducing the limits $+x_0$ and $-x_0$ which are the cut-off points of the integral, equation (9.43) changes to:

$$(2\pi)^{1/2} F(\mu) = \int_{-x_0}^{x_0} \exp(x) f[\exp(x)] \exp(i\mu x)\, \mathrm{d}x + f(x_0, \mu) \tag{9.49}$$

Since the cut-off error of the x_0 limits is reflected in increasing the height of the error ripples in the final results, tending to obscure the real peaks present, it is necessary to choose x_0 in such a way that the value of $f(x_0, \mu)$ is sufficiently small to ensure good resolution. In the same way, the integration limits of equation (9.48), $\pm\mu_0$, affect the eventual frequency spectrum. If μ_0 is chosen too large, the cut off at x_0 causes an increase in the height of the error ripples. On the other hand, if μ_0 is too small, a broadening of the final peaks occurs, resulting in a resolution loss.

For the numerical integration, Gardner *et al.* recommend that all decay constants should be between 0 and 1. Next, each value of $f(t)$ is multiplied by its respective t value and, using the transformation described by equation (9.41), the results are plotted as exp $(x) f[\exp(x)]$ versus x.

The function $F(\mu)$ is subsequently calculated as follows:

$$F(\mu) = [1/(2\pi)^{1/2}] \int_0^{x_0} \{[f^*(x) + f^*(-x)] \cos \mu x + i[f^*(x) - f^*(-x)] \sin \mu x\}\, \mathrm{d}x \tag{9.50}$$

where $f^*(x)$ stands for exp $(x) f[\exp(x)]$. This yields F_r and F_i, respectively the real and imaginary parts of $F(\mu)$. $K(\mu)$ is also composed of a real and an imaginary part, respectively K_r and K_i, since it turns out to be the Euler integral of the complex gamma function:

$$K(\mu) = [1/(2\pi)^{1/2}]\, \Gamma(1 + i\mu) \tag{9.51}$$

Hence one can calculate that equation (9.48) becomes

$$g[\exp(-y)] = \frac{1}{\pi} \int_0^{\mu_0} \left[\frac{F_r K_r + F_i K_i}{K_r^2 + K_i^2} \cos y\mu + \frac{F_i K_r - F_r K_i}{K_r^2 + K_i^2} \sin y\mu \right] \mathrm{d}\mu \tag{9.52}$$

which gives the solution one is looking for.

Since Fourier type transforms are used, one can expect that a certain amount of smoothing will be performed on the statistical scatter of the data. However it should be noted, as for the previous methods, that smoothing prior to analysis appreciably improves the final results.

In general one can remark that it is advantageous to subtract the background and the activity due to isotopes which live long in comparison to the measuring time of the whole decay curve, before starting the analysis. These activities yield a relatively small value for λ and no exact half-life calculation can be performed on these isotopes. On the other hand, analyses of decay curves are seriously hindered, when dealing with low activities and consequently large statistical fluctuations. The reliability of the results will also largely depend on the ratios of the A_j^0 values belonging to the different components of the complex decay curve. It is obvious that the activity in each point of the decay curve is referred to the middle of the measuring interval. When the measuring interval becomes of the same order of magnitude as the half-life of the isotope, substantial errors can occur. Correction for these errors, and for the dead-time of the measuring apparatus are described in Chapter 10.

4. *Optimizing Programs*

It is obvious that computer programs can be used in activation analysis for calculating the induced activity by a nuclear reaction and for determining optimum conditions for irradiation and decay. This can be very useful especially when dealing with complex activation and decay modes as occur in parent-daughter relations and branching activation or decay (see Chapter 5).

The complex program "AARDVARK", which has been described

and $K(\mu)$, which represents the Fourier transform of exp $[-\exp(s)]$ exp (s).

According to this, equation (9.44) can be written:

$$F(\mu) = (2\pi)^{1/2} G(\mu)\, K(\mu) \tag{9.46}$$

from which:

$$G(\mu) = [1/(2\pi)^{1/2}]\,[F(\mu)/K(\mu)] \tag{9.47}$$

Writing the inverse Fourier transform of $G(\mu)$, one eventually finds:

$$g[\exp(-y)] = (1/2\pi) \int_{-\infty}^{\infty} [F(\mu)/K(\mu)] \exp(iy\mu)\, d\mu \tag{9.48}$$

It is obvious however that equations (9.43) and (9.48) cannot be numerically integrated from $-\infty$ to ∞. So, by introducing the limits $+x_0$ and $-x_0$ which are the cut-off points of the integral, equation (9.43) changes to:

$$(2\pi)^{1/2} F(\mu) = \int_{-x_0}^{x_0} \exp(x) f[\exp(x)] \exp(i\mu x)\, dx + f(x_0, \mu) \tag{9.49}$$

Since the cut-off error of the x_0 limits is reflected in increasing the height of the error ripples in the final results, tending to obscure the real peaks present, it is necessary to choose x_0 in such a way that the value of $f(x_0, \mu)$ is sufficiently small to ensure good resolution. In the same way, the integration limits of equation (9.48), $\pm\mu_0$, affect the eventual frequency spectrum. If μ_0 is chosen too large, the cut off at x_0 causes an increase in the height of the error ripples. On the other hand, if μ_0 is too small, a broadening of the final peaks occurs, resulting in a resolution loss.

For the numerical integration, Gardner *et al.* recommend that all decay constants should be between 0 and 1. Next, each value of $f(t)$ is multiplied by its respective t value and, using the transformation described by equation (9.41), the results are plotted as exp $(x) f[\exp(x)]$ versus x.

The function $F(\mu)$ is subsequently calculated as follows:

$$F(\mu) = [1/(2\pi)^{1/2}] \int_0^{x_0} \{[f^*(x) + f^*(-x)] \cos \mu x + i[f^*(x) - f^*(-x)] \sin \mu x\}\, dx \tag{9.50}$$

where $f^*(x)$ stands for exp $(x) f[\exp(x)]$. This yields F_r and F_i, respectively the real and imaginary parts of $F(\mu)$. $K(\mu)$ is also composed of a real and an imaginary part, respectively K_r and K_i, since it turns out to be the Euler integral of the complex gamma function:

$$K(\mu) = [1/(2\pi)^{1/2}]\, \Gamma(1 + i\mu) \tag{9.51}$$

Hence one can calculate that equation (9.48) becomes

$$g[\exp(-y)] = \frac{1}{\pi} \int_0^{\mu_0} \left[\frac{F_r K_r + F_i K_i}{K_r^2 + K_i^2} \cos y\mu + \frac{F_i K_r - F_r K_i}{K_r^2 + K_i^2} \sin y\mu \right] d\mu \tag{9.52}$$

which gives the solution one is looking for.

Since Fourier type transforms are used, one can expect that a certain amount of smoothing will be performed on the statistical scatter of the data. However it should be noted, as for the previous methods, that smoothing prior to analysis appreciably improves the final results.

In general one can remark that it is advantageous to subtract the background and the activity due to isotopes which live long in comparison to the measuring time of the whole decay curve, before starting the analysis. These activities yield a relatively small value for λ and no exact half-life calculation can be performed on these isotopes. On the other hand, analyses of decay curves are seriously hindered, when dealing with low activities and consequently large statistical fluctuations. The reliability of the results will also largely depend on the ratios of the A_j^0 values belonging to the different components of the complex decay curve. It is obvious that the activity in each point of the decay curve is referred to the middle of the measuring interval. When the measuring interval becomes of the same order of magnitude as the half-life of the isotope, substantial errors can occur. Correction for these errors, and for the dead-time of the measuring apparatus are described in Chapter 10.

4. *Optimizing Programs*

It is obvious that computer programs can be used in activation analysis for calculating the induced activity by a nuclear reaction and for determining optimum conditions for irradiation and decay. This can be very useful especially when dealing with complex activation and decay modes as occur in parent-daughter relations and branching activation or decay (see Chapter 5).

The complex program "AARDVARK", which has been described

by Isenhour, [illegible]ns and Morrison (43, 44) does not consider these special cases, but nevertheless can be of great help to the analyst. The master program consists of three subprograms: "OPTIMIZE", "OPTIPLOT" and "MULTIOPT", which can be used either in combination or separately. The program allows the analyst to determine optimum conditions for irradiation and decay time for single and multi element analyses.

All three programs are based on maximizing R_j, which represents the ratio of the activity, induced in an element j, to the activity induced in all elements present. R_j is maximized as a function of irradiation time t_b and decay time t. Indeed R_j can be represented by:

$$R_j = \frac{z_j N_j \varphi_j \sigma_j [1 - \exp(-\lambda_j t_b)] \exp(-\lambda_j t)}{\sum_i z_i N_i \varphi_i \sigma_i [1 - \exp(-\lambda_i t_b)] \exp(-\lambda_i t)} \qquad (9.53)$$

where z represents the detector efficiency in the considered energy region corrected for the possible branching in the decay scheme, N is the number of target nuclei, φ the neutron flux, σ the reaction cross section and λ the decay constant of the formed nucleus.

R_j is subsequently maximized with respect to t_b and t as follows:

$$\left[\frac{\partial R_j}{\partial t_b}\right]_t = 0 \quad \text{and} \quad \left[\frac{\partial R_j}{\partial t}\right]_{t_b} = 0 \qquad (9.54)$$

The master program initiates the operations by reading the input data and subsequently turns control over to each of the subprograms. "OPTIMIZE" firstly determines if the activity produced by a given reaction is sufficient for analysis. For the reactions where this requirement is met, the values for t_b and t are computed according to equation (9.54), in order to obtain a maximum R_j. So this program calculates the optimum conditions for a single element activation in a multicomponent matrix. The programs "OPTIPLOT" and "MULTIOPT" are used for multielement activation analysis in a multicomponent matrix. "OPTIPLOT" computes optimum decay times for a series of irradiation times and then plots the maximum R_j values as a function of irradiation time. These graphical results allow the operator to establish which elements can be simultaneously analyzed for a fixed irradiation time.

The program "MULTIOPT" firstly finds out whether an irradiation time exists for which all considered reactions produce an activity high enough to give rise to R_j values above a fixed minimum. Therefore, decay time optimization is applied. Then, the most limiting reaction is disregarded, and the program starts all over again with the remaining reactions. The discarded reaction is still taken into account for the calculations, along with all other interferences. The process is repeated until only two reactions remain under consideration. In this way "MULTIOPT" indicates which combination of elements can be analyzed for one fixed irradiation time. The program was applied by Isenhour *et al.* (43,44) to the analysis of impurities in high purity silicon samples. The results of "OPTIMIZE" and "MULTIOPT" are summarized in Table 9.6 whereas Figure 9.15 shows the graph of the maxi-

TABLE 9.6

Results of "OPTIMIZE" and "MULTIOPT" programs for the analysis of a 1 g silicon sample (43)

	OPTIMIZE Section				
Reaction used	Maximum ratio $(R_j)_{max}$	Optimum irradiation time	Optimum decay time	Activity produced (dps)	Weight (μg)
^{75}As (n, γ) ^{76}As	0.242	17.4 h	70.2 h	20	0.02
^{63}Cu (n, γ) ^{64}Cu	0.267	1.7 h	23.5 h	20	0.05
^{65}Cu (n, γ) ^{66}Cu	—	—	—	<20	0.05
^{71}Ga (n, γ) ^{72}Ga	0.038	47.3 h	18.3 h	20	0.005
^{41}K (n, γ) ^{42}K	—	—	—	<20	0.05
^{55}Mn (n, γ) ^{56}Mn	0.890	52.6 m	3.0 h	684	0.05
^{23}Na (n, γ) ^{24}Na	0.999	48.0 h	84.0 h	20	0.34
^{121}Sb (n, γ) ^{122}Sb	0.768	36.5 h	7 d	24.3	0.03
^{181}Ta (n, γ) ^{182}Ta	—	—	—	<20	0.05
^{64}Zn (n, γ) ^{65}Zn	—	—	—	<20	2.0
^{68}Zn (n, γ) ^{69}Zn	0.279	7.25 h	29.0 h	38.8	2.0

	MULTIOPT Section						
Minimum ratio	Irradiation time (hour)	^{56}Mn	^{24}Na	^{122}Sb	^{65}Zn	^{64}Cu	^{76}As
0.239	37.6	2.4	82.3	168.0	24.2	16.6	63.3
0.257	22.7	2.4	77.3	147.7	25.7	18.1	—
0.276	22.7	2.4	77.3	147.7	25.7	—	—
0.754	48.0	2.4	84.0	168.0	—	—	—
0.890	1.1	3.0	22.0	—	—	—	—

mum activity ratio versus irradiation time obtained by the program "OPTIPLOT". From Figure 9.15 it can be seen that for a 30 h irradiation time, and applying optimum decay times, sodium, manganese and antimony can be analyzed with good precision; for zinc, copper and arsenic the situation is less favorable. This is sustained by the results of "MULTIOPT" from which it appears that for a 37 h irradiation all six elements obtain a R_f ratio of at least 0.239.

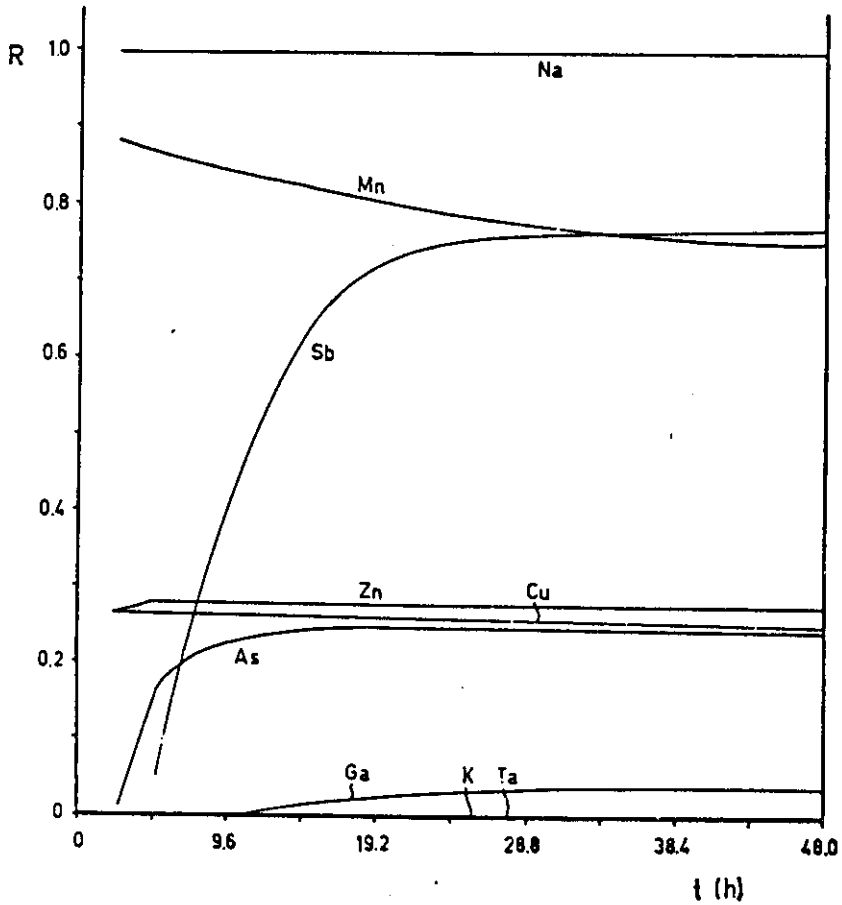

Fig. 9.15. Optiplot results for 1 g silicon matrix containing 0.02 μg As, 0.05 μg Cu, 0.005 μg Ga, 0.05 μg K, 0.34 μg Na, 0.03 μg Sb, 0.05 μg Ta, 2 μg Zn, 0.05 μg Mn (43).

(D) Use of Special Detection Systems

The analysis of complex gamma spectra can be highly simplified when one succeeds in suppressing the Compton region of the spectra. Two ways of obtaining this result exist:

surrounding the NaI(Tl) detector with an anticoincidence shield;

subtracting the Compton continuum of the NaI(Tl) spectrum by means of a second detector, which gives rise to Compton effect only.

The principles of both methods have been discussed in Chapter 6.

Perkins (45,46,47) used two 12.7 × 12.7 cm cylindrical NaI(Tl) detectors, between which the source was sandwiched. The detectors were surrounded by an NaI(Tl) scintillator in anticoincidence. The spectrometer used was a 4096 channel multiparameter analyzer. With this anticoincidence shield, the already small Compton continuum was further reduced by a factor of about 5. Furthermore, cascade gammas were easily measured by means of a sum coincidence technique, and used for quantitative determination. The author determined simultaneously and without chemical separations the isotopes ^{60}Co, ^{22}Na, ^{88}Y and ^{134}Cs in "fall-out" products, and ^{64}Cu, ^{72}Ga, ^{76}As, ^{140}La, ^{140}Ba, ^{124}Sb and ^{60}Co in reactor cooling water.

The Compton subtraction spectrometer, as firstly described by Peirson and Iredale (48,49,50) was applied by the last author for the determination of iron, gadolinium, sodium and scandium in aluminium. The reactions used together with the obtained limits are represented in Table 9.7.

TABLE 9.7

Detection limits for the analysis of impurities in aluminium after Irodale (51)

Reaction	Detection limit (ppm)
^{58}Fe (n, γ) ^{59}Fe	1.2
^{71}Ga (n, γ) ^{72}Ga	530
^{45}Sc (n, γ) ^{46}Sc	0.5
^{23}Na (n, γ) ^{24}Na	10

Adams and Hoste (52) determined by means of a Compton subtraction spectrometer antimony in lead in a concentration region from 1 to 0.03%, using the 0.566 MeV gamma ray of ^{122}Sb. In order to correct for matrix shielding and flux variations, a known amount of gold was

spotted on the samples and the 0.412 MeV gamma ray of ^{198}Au was used as an internal standard.

De Soete and Hoste (53) describe the determination of cobalt in nickel by means of a modified Compton subtraction spectrometer (54,55). The isotope ^{60}Co formed by (n, γ) reaction on the element to be determined is measured versus the ^{58}Co activity produced by (n, p) reaction on the nickel matrix, which is used as an internal standard. By choosing an adequate irradiation facility with a suitable thermal to fast flux ratio, cobalt concentrations ranging from 10^4 to 0.5 ppm could be determined nondestructively in a nickel matrix. The limit of the method is due to the reaction ^{60}Ni(n, p)^{60}Co.

The application of large NaI(Tl) crystals can be useful for the suppression of the Compton spectrum, although generally an appreciable loss in resolution obtains. Thin NaI(Tl) wafers, however, are advantageous for the measurement of X-rays and low energy gamma rays, in the presence of high energy radiation.

Indeed, a 1 mm thick NaI(Tl) wafer is practically transparent for gamma rays above 150 keV, whereas good detection efficiency still occurs for 100-keV photons. Gijbels and Hoste (56) made use of a 7.5 cm diameter by 0.1 cm thickness wafer, provided with a beryllium window of 37 mg per cm^2 for the determination of traces of osmium in ruthenium. Osmium was measured as ^{191}Os ($T_{1/2}$=16 d), emitting an iridium X-ray at 65 keV. The ruthenium matrix mainly gives rise to ^{103}Ru ($T_{1/2}$=40 d), with its main gamma ray at 0.498 MeV. Although the osmium was separated from the ruthenium activity by distillation from H_2SO_4–H_2O_2, the osmium fraction appeared to be contaminated with ^{103}Ru. However, the wafer-detector allowed the determination of 10 ppm osmium in a 10 mg ruthenium sample, without need for correction due to the ^{103}Ru activity.

The development of the Ge(Li) detector constituted the biggest step forward in gamma ray spectroscopy, resulting in a resolution gain by a factor of approximately 20 in comparison with the NaI(Tl) detectors. These semiconductors described in Chapter 6, section III, A, 3, simplify chemistry to group separations, as numerous isotopes can be determined in one single measurement.

(E) Automated Activation Analysis

Automated activation analysis can start with the irradiation and end with the print out of the results. Automation can be worthwhile

when dealing with the analysis of certain elements in large sample series such as minerals, oil, steel and biological materials. The technique can be developed so as to obtain a push button machine which can be operated by unspecialized personnel.

The system consists of the following components:

the irradiation source, a neutron generator, a nuclear reactor, an accelerator, . . . ;

a transport system for the samples;

if needed, automated chemical separations;

adequate measuring techniques, tending towards specificity;

a computing machine for data analysis and evaluation of the results;

a programming system which controls the different operations.

When a neutron generator can be used for irradiation purposes, the costs of the installation may be kept within reasonable limits. However, when a nuclear reactor or a powerful accelerator is needed, costs are quite high, so that only important research centres can use such a system economically, e.g. a centre for activation analysis, for oil research, for geological prospecting or for agricultural research.

The well known work of Wainerdi and coworkers (57,58,59,60) deals with automated activation analysis systems using a nuclear reactor as irradiation source. The apparatus is capable of performing 750,000 analyses per year and was used, e.g. for the simultaneous and non-destructive determination of sodium, chlorine and magnesium in blood serum (61). Further applications were made in the determination of tellurium in blood, urine and water, selenium in urine and blood, and silver in brain tissue of rats (62). In this last analysis, the total computer time per sample was 2.6 m and the cost was estimated by the authors as 1.37 $ per analysis.

Hoste *et al.* (63) describe an automated oxygen analysis system for steel samples, using 14 MeV neutrons from a neutron generator to produce the reaction ^{16}O(n, p)^{16}N ($T_{1/2}$ = 7.4 s). A rectangular double pneumatic transport system for cylindrical 40 g steel samples 9 mm × 26 mm diameter is used, allowing the standard to be activated at the same time as, and behind the sample. The ^{16}N gamma activities above 4.5 MeV are measured by means of two separate counting systems. The data are fed into a small electronic computer, which calculates and prints the oxygen content in mg. The sensitivity of the method is about 0.1 mg oxygen at maximum neutron output.

The complete system is industrialized and is operational in a steel

plant on a 24 r basis, with up to 400 analyses per day. Starting from the liquid steel bath, the oxygen content is obtained within less than 5 m. As an extension, the authors studied oxygen analyses in 11 different nonferrous metals: Al, Bi, Cd, Co, Cu, Nb, Pb, Ta, Ti, Zn and Zr. Next to the well known interference, due to the reactions $^{11}B(n,p)^{11}Be$ ($T_{1/2}$ = 13.6 s) and $^{11}B(n,\alpha)^{8}Li$ ($T_{1/2}$ = 0.85 s), possible matrix interferences of these metals on the determination were investigated. Lead and zirconium interfere seriously by the formation of the respective isotopes ^{207m}Pb ($T_{1/2}$ = 0.8 s) and ^{90m}Zr ($T_{1/2}$ = 0.8 s), whereas copper and aluminium interfere to a lesser degree, mainly due to pile-up of the induced matrix activity. All of these interferences could be eliminated by the choice of proper measurement sequences.

Comar and Le Poec (64,65) constructed an automated system for the separation and determination by activation analysis of iodine in biological materials. The produced isotope ^{128}I is automatically purified by anion exchange, extracted and distilled. A metering pump transfers the iodine fraction in a spiral, placed between two beta detectors. The results of the measurements are clearly printed.

Examples of automated chemical separation techniques are given in Chapter 8.

References

1. Adams, F., and Hoste, J., *At. En. Rev.*, 4(2), 113 (1966).
2. Münzel, H., *I.A.E.A., Radiochem. Meth. of Anal.*, Salzburg, Proc. II, p. 141 (1964).
3. Cumming, J. B., *Nucl. Sci. Series Rept.* NAS-NS 3107, p. 25 (1962).
4. Nervik, W. E., *Nucl. Sci. Series Rept.* NAS-NS 3107, p. 9 (1962).
5. Gardner, D. G., Gardner, J. C., Laush, G., and Meinke, W. W., *Journ. of Chem. Phys.*, 31(4) 978 (1959).
6. Shafer, R. E., *Nucl. Sci. Series Rept.* NAS-NS 3107, p. 41 (1962).
7. Croall, I. F., *Rept. AERE-R/4227* (1963).
8. Korthoven, P. J. M., and Carlsen, F. S., Rept. IS-1501, TID-4500, Ames Lab. at Iowa State University (1966).
9. Aubouin, G., *Radiochim. Acta*, 1(3), 117 (1963).
10. Gibbons, D., and Lawson, D., *Mod. Trends in Activation Anal.*, Texas, Proc. p. 172 (1965).
11. Adams, F., Hoste, J., and Speecke, A., *Talanta*, 10, 1243 (1963).
12. Dams, R., and Hoste, J., *Anal. Chim. Acta*, 41, 205 (1968).
13. Borg, D. C., Segel, R. E., Kienle, P., and Campbell, L., *J.A.R.I.*, 11, 10 (1961).
14. Hecker, R., and Herr, W., *Nukleonik*, 4(1), 19 (1962).
15. Salmon, L., *AERE Report C/R* 2377(3) (1957).
16. Kim, J. I., and Hoste, J., *Anal. Chim. Acta*, 33, 449 (1965).
17. Adams, F., and Hoste, J., *Acta Chimica Academiae Scientiarum Hungaricae*, 52(2), 115 (1967).
18. Wölfle, R., Herpers, V., and Herr, W., *Z. für Anal. Chem.*, 233(4), 241 (1968).
19. Kim, J. I., Speecke, A., and Hoste, J., *Anal. Chim. Acta*, 33, 123 (1965).
20. Adams, F., and Hoste, J., *Nucleonics*, 22, 55 (1964).
21. Wahlgren, M., Wing, J., and Hines, J., *Mod. Trends in Act. Anal.*, Texas, Proc. p. 134 (1965).
22. Helmer, R. G., Heath, R. L., Smittroth, L. A., Jayne, G. A., and Wagner, L. M., *Nucl. Instr. and Meth.*, 47, 305 (1967).
23. Bock-Werthmann, W., and Schulze, W., *Mod. Trends in Act. Anal.* Texas, Proc., p. 145 (1961).
24. Guinn, V. P., and Lash, J. E., *Nucl. Sci. Series Rept.* NAS-NS 3107, p. 243 (1962).
25. Broadhead, K. G., Shanks, D. E., and Heady, H. H., *Mod. Trends in Activ. Anal.*, Texas, Proc., p. 39 (1965).
26. Van Grieken, R., Gijbels, R., Speecke, A., and Hoste, J., *Anal. Chim. Acta*, 43, 199 (1968).
27. De Neve, R., De Soete, D., and Hoste, J., *Anal. Chim. Acta*, 40, 379 (1968).
28. Op de Beeck, J., and Hoste, J., *Anal. Chim. Acta*, 35, 427 (1966).
29. O'Kelley, G. D., *Nucl. Sci. Series Rept.* NAS-NS 3107 (1962).
30. Savitzky, A., and Golay, M. J. E., *Anal. Chem.*, 36(8), 1627 (1964).
31. Yule, H. P., *Anal. Chem.*, 38(1), 103 (1966).
32. Yule, H. P., *Nucl. Instr. and Meth.*, 54, 61 (1967).
33. Op de Beeck, J., Ghent University, Belgium; private communication.
34. Scofield, N. E., *U.S. Naval Radiolog. Defence Lab.*, Rept. USNRDL-TR, 447 (1960).
35. Zerby, C. D., and Moran, H. S., *USAEC Rept.*, ONRL-3169 (1962).
36. Heath, R. L., *AEC Research and Development Rpt.* IDO-16880-1, TID-4500 1 (1964).
37. Helmer, R. G., Heath, R. L., Metcalf, D. D., and Cazier, G. A., IDO-17015 (1964).
38. Salmon, L., *Nucl. Instr. and Meth.*, 14, 193 (1961).
39. Ferguson, A. J., *AECL*-1398 (1961).
40. Heath, R. L., *Proc. of the 8th Scintillation and Solid State Counter Symp., IRE Trans. on Nucl. Sci.*, NS-9, 3, 294 (1962).
41. Hooke, R., and Jeeves, T. A., *J. Assoc. Comp. Mach.*, 8, 222 (1962).
42. Wilde, D. J., *Optimum Seeking Methods*, Prentice Hall, p. 145 (1964).
43. Isenhour, T. L., Evans Jr., C. A., and Morrison, G. H., *Modern Trends in Act. Anal.*, Texas, Proc. p. 123 (1965).
44. Isenhour, T. L., and Morrison, G. H., *Anal. Chem.*, 36, 1089 (1964).
45. Perkins, R. S., *et al.*, *Rev. Sci. Instr.*, 31, 24 (1960).
46. Perkins, R. S., *Mod. Trends in Act. Anal.*, Texas, Proc. p. 50 (1961).
47. Perkins, R. S., *I.A.E.A., Radiochem. Meth. of Anal.*, Salzburg, Proc. II, p. 47 (1964).
48. Peirson, D. H., *Nature*, 173, 990 (1954).

49. Peirson, A., *Brit. J. Appl. Phys.*, 6, 444 (1955).
50. Peirson, D. H., and Iredale, P., *Brit. J. Appl. Phys.*, 8, 422 (1957).
51. Iredale, P., *AERE-EL/M*-108 (1960).
52. Adams, F., and Hoste, J., *Talanta*, 9, 827 (1962).
53. De Soete, D., and Hoste, J., *I.A.E.A., Radiochem. Meth. of Anal.*, Salzburg, Proc. II, p. 91 (1964).
54. De Soete, D., and Hoste, J., *Nature*, 194, 859 (1962).
55. De Soete, D., and Hoste, J., *Radiochim. Acta*, 4, 35 (1965).
56. Gijbels, R., and Hoste, J., *Anal. Chim. Acta*, 29, 289 (1963).
57. Gibbons, D., Fite, L. E., and Wainerdi, R. E., *Anal. Chem.*, 34, 269 (1962).
58. Kuykendall, W. E., Wainerdi, R. E., and associates; I.A.E.A. *Use of Radioisotopes in the Phys. Sci. and Ind.*, Copenhagen RICC/198 (1960).
59. Wainerdi, R. E., and du Beau, N. P., *Science*, 139, 1027 (1963).
60. Wainerdi, R. E., Fite, L. E., Gibbons, D., Wilkins, W. W., Jiminez, P. and Drew, D., I.A.E.A., *Radiochem. Meth. of Anal.*, Salzburg, Proc. II, p. 149 (1964).
61. Drew, D., Fite, L. E., and Wainerdi, R. E., *Nucl. Sci. Series Rept.* NAS-NS 3107, p. 237 (1962).
62. Wainerdi, R. E., Fite, L. E., and Steele, L. E., 3e Congrès Int. de Biologie de Saclay, Comptes-rendus, p. 171 (1963).
63. Hoste, J., De Soete, D., and Speecke, A., *Euratom Rept.*, EUR 3565e (1967).
64. Comar, D., and Le Poec, C., *Mod. Trends in Act. Anal.*, Texas, Proc. p. 351 (1965).
65. Comar, D., and Le Poec, C., I.A.E.A. *Radiochem. Meth. of Anal.*, Salzburg, Proc. II, p. 15 (1964).

CHAPTER 10

SYSTEMATIC ERRORS IN ACTIVATION ANALYSIS

I. General Considerations

The activity induced in an element after an irradiation time t_b can be calculated from equation (5.36), in the case of "simple activation". A more practical form of this equation is

$$R(t_b) = \frac{wz\theta N_A \sigma\varphi y}{A}\left[1 - \exp\left(\frac{-0.693\, t_b}{T_{1/2}}\right)\right] \qquad (10.1)$$

$R(t_b)/3.7 \times 10^7$ gives the activity in millicurie (mc). After a waiting time t, the activity is obviously given by equation (5.37):

$$R(t_b, t) = R(t_b) \exp\left(-0.693\, t/T_{1/2}\right) \qquad (10.2)$$

In the case of more complex systems, including isomeric activation, parent-daughter relationships, etc. equations (5.44), (5.47), (5.52), (5.53), (5.55), (5.56), (5.59), (5.60) ... or their practical equivalents should be used. In the above equations:

- R = measured activity in cps ($R = zD$, where D = disintegration rate in dps);
- w = weight of the irradiated element in gram; (if a compound, such as an oxide, is irradiated, its weight must be multiplied with the appropriate analytical conversion factor);
- z = efficiency of the detector;
- θ = abundance of the activated nuclide (100% = 1);
- A = atomic weight of the irradiated element;
- N_A = Avogadro's number = 6.023×10^{23};
- y = chemical yield (if the activity is counted after a chemical separation);
- $T_{1/2}$ = half-life of the radionuclide formed;
- t_b and t = irradiation and waiting time respectively; (expressed in the same unit as $T_{1/2}$: s, m, h ...);
- σ = isotopic activation cross section. If only thermal activation occurs (i.e. at the irradiation position the cadmium ratio of